

Fabrication of Silver Nanoparticles Supported on Rice Straw: *In Vitro* Antibacterial Activity and its Heterogeneous Catalysis in the Degradation of 4-Nitrophenol

Roshanak Khandanlou,^{a,*} Gek Cheng Ngoh,^{a,*} Wen Tong Chong,^b Saadi Bayat,^c and Elnaz Saki^d

To investigate the influence of pH on the size and distribution of silver nanoparticles (Ag-NPs) as well as the antibacterial activity and catalytic performance of rice straw/silver nanocomposites (RS/Ag-NCs), Ag-NPs were synthesized on the surface of rice straw (RS) with various percentages of Ag-NPs (1.0, 5.0, 10.0, and 20.0 wt.%) under different temperatures and diverse pH values. The ultraviolet-visible spectroscopy of synthesized RS/Ag-NCs became noticeable with increased pH, and the peaks were blue-shifted to lower wavelengths. X-ray powder diffraction (PXRD) demonstrated the presence of pure Ag-NPs. Transmission electron microscopy (TEM) showed that the diameters of Ag-NPs on RS were between 7.78 and 2.84 nm at pH values of 8 to 10. The antibacterial activity of various sizes of Ag-NPs on RS was examined using Gram-negative bacteria (*Escherichia coli*) and Gram-positive bacteria (*Staphylococcus aureus*) based on the well diffusion technique. Higher antibacterial activity was detected as the loading percentage of RS/Ag-NCs increased and particle size decreased. The superior catalytic performance of 20.0 wt.% RS/Ag-NCs was considered in a test reaction in 4-nitrophenol (4-NP) reduction in the presence of sodium borohydride (NaBH₄) in an eco-friendly solvent at ambient temperature. The results represented the high-performance catalytic activity of 20.0 wt.% RS/Ag-NCs.

Keywords: Silver nanoparticles; Rice straw; Antibacterial activity; Catalytic performance; Transmission electron microscopy; X-ray powder diffraction

Contact information: a: Department of Chemical Engineering, Faculty of Engineering, University of Malaya, 50603, Kuala Lumpur, Malaysia; b: Department of Mechanical Engineering, Faculty of Engineering, University of Malaya, 50603, Kuala Lumpur, Malaysia; c: Institute of Molecular Sciences (LIMS), La Trobe University, 3086, Melbourne, Australia; d: Department of Pathology, Faculty of Medicine and Health Sciences, University Putra Malaysia, 43400, UPM Serdang, Selangor, Malaysia;

* Corresponding authors: roshanak_bch@yahoo.com, ngoh@um.edu.my

INTRODUCTION

Lignocellulosic biomass is a composite of cellulose (a glucose polymer), hemicellulose (a sugar heteropolymer), and lignin (a non-fermentable phenyl-propene unit polymer) (Mohanram *et al.* 2015). Rice is one of the most important agricultural products in the world, with a reported global production of 731 million tons per year (Binod *et al.* 2010). Rice straw (RS) is an agricultural by-product of rice production that is generated in large quantities but is not effectively used. Most rice straw is disposed of in landfills or by burning, resulting in environmental issues. As RS is inexpensive and readily available,

there have been several attempts to devise efficient uses for it (Oberoi *et al.* 2012; Kurokochi and Sato 2015). Nanotechnology is an emerging field that deals with the synthesis, strategy, and manipulation of particle structures ranging from 1 nm to 100 nm (Ibrahim 2015). Within this size range, the chemical, physical, and biological properties change fundamentally in terms of both individual atoms or molecules and their corresponding bulk. Novel applications of nanoparticles and nanomaterials have been growing rapidly in various industries because of their completely new or enhanced properties based on size, distribution, and morphology (Ibrahim 2015).

Metal nanoparticles have unique optical, magnetic, and catalytic properties, which can be tuned by controlling their size, shape, and chemical composition (Kelly *et al.* 2003). Noble metal nanoparticles, silver nanoparticles in particular, exhibit strong localized surface plasmon resonance (LSPR) absorption of visible light and have applications in plasmonics (Tao *et al.* 2007), catalysis (Rashid and Mandal 2007), biodiagnostics (Rosi and Mirkin 2005), nanophotonics (Shrivastava *et al.* 2009), and optical biosensing (Riboh *et al.* 2003). Ag-NPs are potentially applicable in the biomedical and food packaging fields because of their unique biological and physicochemical properties, such as broad antimicrobial activity and heat stability (Sondi and Salopek-Sondi 2004; Kanmani and Rhim 2014). The antimicrobial activity of Ag-NPs depends on their composition, size, shape, chemical functionality, and surface charge, which are greatly influenced by their preparation method (Martinez-Castanon *et al.* 2008). Therefore, a proper synthesis method in which morphology, size, stability, toxicity, and other properties are controlled is essential. There are a number of Ag-NPs preparation methods including chemical reduction and physical methods such as laser ablation, microwave dielectric heating, ultrasonic irradiation, and radiolysis (Shankar and Rhim 2015). The antimicrobial properties of silver ions have been exploited in catheters, burn wounds, and dental work (Kim *et al.* 2007). Silver-containing materials and coatings with antimicrobial activity reduce infection in hospitals (Gosheger *et al.* 2004; Rupp *et al.* 2004). Fibers containing silver nanoparticles could be utilized to eradicate microorganisms on textile fabrics (Jeong *et al.* 2005). They also display a strong cytoprotective activity toward HIV-infected cells (Sun *et al.* 2005a).

Nitro compounds are generally produced as by-products in different commercial industries such as agrochemicals, dyes, and pharmaceuticals (Gazi and Ananthakrishnan 2011). Aromatic amines are essential starting materials and intermediates for the fabrication of various chemicals. Among different nitro-compounds, 4-nitrophenol (4-NP) is one of the most frequent by-products, and it is toxic to the environment (Solanki and Murthy 2011; Davarpanah and Kiasat 2013). In some manufacturing industries, 4-aminophenol (4-AP) is derived from 4-nitrophenol (4-NP) through reduction. 4-AP is a precursor necessary for different drugs such as acetaminophen, phenacetin, acetanilide, *etc.*

Previous studies also used different types of catalyst for reduction of 4-NP in the presence of sodium borohydride. For example, Jana *et al.* (2006) used silver nanoshell-coated cationic polystyrene beads for the reduction of 4-NP in the presence of sodium borohydride. Saha *et al.* (2009) have grown silver and gold nanoparticles on calcium alginate gel beads to use as a catalyst for reduction of 4-NP to 4-AP using sodium borohydride. They found that the as-prepared catalysts are very efficient, stable, easy to prepare, eco-friendly, cost-effective, and they have the potential for industrial applications. Wang *et al.* (2015) studied the effect of Ag-NPs on tea polyphenols-modified graphene as a catalyst toward the reduction of 4-NP by sodium borohydride. Their results showed that this nanohybrid, combining the unique catalytic properties of Ag-NPs with the excellent adsorption and electron transfer ability of graphene, exhibited enhanced catalytic activity

for reduction of 4-NP by sodium borohydride. Zheng *et al.* (2015) synthesized Ag@guar gum (Ag@GG) beads and studied the catalytic activity for reduction of 4-NP to 4-AP in the presence of excess borohydride. The results indicated at these crosslinked Ag@GG beads show excellent catalytic performance for the reduction of 4-NP within 20 min.

Today, approaches using renewable natural resources have attracted increasing attention due to its availability, biodegradability, non-toxicity, and low cost. There have been numerous reports about the synthesis of Ag-NPs supported on various matrixes such as graphene oxide (De Faria *et al.* 2014), starch (Mohan *et al.* 2016; Das *et al.* 2015), glassy carbon (Khan *et al.* 2016), montmorillonite/starch (Shabanzadeh *et al.* 2015), *etc.* The present work is the first time RS has been used as a by-product of rice to support the Ag-NPs in which the properties of RS/Ag-NCs were improved and have potential in different areas. For example RS/Ag-NCs can be used in removal of heavy metals because the RS is used in heavy metals adsorption and the loading of Ag-NPs on the RS surface improve the adsorption. On the other hand Ag-NPs have antibacterial activity, which is useful for several applications. Therefore, due to the high antibacterial activity of RS/Ag-NCs, they can be applied in the packaging industry. Also, using RS/Ag-NCs as a catalyst for reduction of 4-NP to 4-AP in the presence of sodium borohydride is a new research topic in the area of catalytic activity which is significant and adds value for further research.

In this study, RS/Ag-NCs were prepared with various Ag-NPs percentages under constant temperature and different pH values with the use of sodium hydroxide as a reducing agent. The effect of pH on the size and distribution of Ag-NPs and the effect of Ag-NPs size on the antibacterial activity of RS/Ag-NCs were investigated. In addition, the catalytic activity of 20.0 wt.% RS/Ag-NCs was evaluated for their ability to reduce the aromatic nitro groups (4-NP) into non-toxic aromatic amine groups (4-AP) in the water in the presence of sodium borohydride.

EXPERIMENTAL

Materials

RS was collected from a native field (Bukit Tinggi, Kedah, Malaysia). The following chemical reagents were of analytical grade and used without further purification: AgNO₃ (99.89%, Merck, Frankfurter, Germany); NaOH (99.0%, Merck, Darmstadt, Germany); urea (99%, Hamburg Chemicals, Hamburg, Germany); HCl (37.0%, Sigma-Aldrich, St Louis, MO, USA); HNO₃ (70.0%, Sigma-Aldrich); sodium borohydride (NaBH₄, ≥98.0%, Sigma-Aldrich); and 4-nitrophenol (4-NP, 99.0%, Sigma-Aldrich).

Preparation of Rice Straw/Silver Nanocomposites

The RS/Ag-NCs were prepared with 1.0, 5.0, 10.0, and 20.0 wt.% Ag-NPs in 2 g of RS. For preparation of RS/Ag-NCs, 2 g of RS was suspended in distilled water, and 2 M urea was poured into these mixtures. Various volumes of AgNO₃ salt were then added to the suspensions under vigorous stirring. The suspensions were heated at 70 °C, and 1.0, 5.0, 10.0, or 20.0 mL of 2 M NaOH was added. The mixture was continuously stirred for 1 h. The preparation of Ag-NPs was performed at basic pH, which was controlled throughout the reaction procedure. The pH of the RS and urea suspension was 5.71; after adding AgNO₃ and NaOH, the pH of the suspension was between 8 and 10. The prepared RS/Ag-NC was centrifuged, washed with distilled water and ethanol until the silver ion residue was removed, and dried in an oven at 60 °C.

Antibacterial Activity

The *in vitro* antibacterial activity of the prepared samples was assessed by using the well diffusion technique in Muller-Hinton agar (MHA), and the estimation of the inhibition zone in millimeters (mm) was based on the recommended standards of the Clinical and Laboratory Standards Institute (CLSI). Examples of some standards are as follows: (ISO 16256 (2012); ISO 16782 (2012); ISO/NP 20776-1 (2015); ISO 20776-1 (2006); ISO 20776-2 (2007); ISO 17511 (2003); ISO/NP TS20914 (2015)).

The antibacterial resistance of RS/Ag-NCs was examined in the pathogenic Gram-positive bacteria *Staphylococcus aureus* (*S. aureus*) and the Gram-negative bacteria *Escherichia coli* (*E. coli*) at various Ag-NPs sizes and percentages. The clinical strains of pathogenic bacteria were obtained from Serdang Hospital, Malaysia. Briefly, bacterial strain stock cultures were maintained at 4 °C in MHA medium. Approximately 20 mL of sterile MHA medium was poured into sterile petri plates. Triplicates of the plates were swabbed with the overnight bacterial cultures (10⁸ cells/mL).

After the agar hardened, wells with a diameter of 7 mm were cut using a sterile cork borer. Lastly, the stock NPs samples (50 µg/mL) were added to each well. In addition, RS, which was employed as a matrix for Ag-NPs, was used as a negative control. A stock solution of AgNO₃ was applied as a positive control with the same concentration (50 µg/mL) for the purpose of comparison and then incubated at 37 °C. After 24 h, the inhibition zone was measured.

Catalytic Activity Examination

In the RS/Ag-NCs-catalyzed 4-nitrophenol (4-NP) hydrogenation reaction, 20.0 wt.% of RS/Ag-NCs was added to 5 mL of a solution containing 60 mg of 4-NP (0.43 mmol, 1 eq), 180 mg of NaBH₄ (4.75 mmol, 3 eq), and 6 mg of catalyst. The reaction mixture was sonicated and monitored using a UV-Vis spectrophotometer in the wavelength range of 210 to 600 nm every 3 min. The characteristic maximum absorbance of 4-NP at 400 nm was utilized to indicate the 4-NP remaining, and the absorbance at 297 nm was used to identify the product (4-aminophenol).

Characterization of Ag-NPs

Electron field-emission scanning electron microscopy (FESEM) with energy-dispersive X-ray fluorescence (EDXF) spectroscopy was used to examine the morphology of samples. A JEOL JSM-7600F instrument was used (Tokyo, Japan). Transmission electron microscopy (TEM) with a LEO 906E electron microscope (Jena, Germany) was used to calculate the size and morphology of the prepared samples. The distribution of particle size was established using version 3.00 of the UTHSCSA Image Tool software (San Antonio, TX, USA).

Powder X-ray diffraction (PXRD) with Cu K α radiation using a D8 Advance X-ray diffractometer (Bruker AXS, Billerica, Massachusetts, USA) was carried out to ascertain the purity of the Ag-NPs.

The UV-visible spectra were detected in the range of 300 to 700 nm using a PerkinElmer Lambda 25 UV-visible spectrophotometer (Waltham, Massachusetts, USA). Fourier transform infrared spectroscopy (FT-IR) was conducted with a Series 100 PerkinElmer FT-IR 1650 spectrophotometer (Waltham, Massachusetts, USA) in the range of 400 to 4000 cm⁻¹.

RESULTS AND DISCUSSION

UV-Visible Spectroscopy

The UV-Vis spectroscopic technique could be used to detect morphological changes, noting that silver nanoparticles having various shapes exhibit surface plasmon resonance (SPR) bands at different frequencies. Figure 1 compares the UV-Vis spectra of suspensions with various pH and Ag-NPs loading. As the pH increased from 8.34 to 10.83, silver bands were detected at 405 to 413 nm (Fig. 1). These absorption bands were attributed to Ag-NPs smaller than 10 nm (Shameli *et al.* 2010b), and they are conventional plasmon bands for spherical or nearly spherical silver particles. There was no Ag-NPs absorption before the addition of NaOH to the RS sample (Fig. 1(a)).

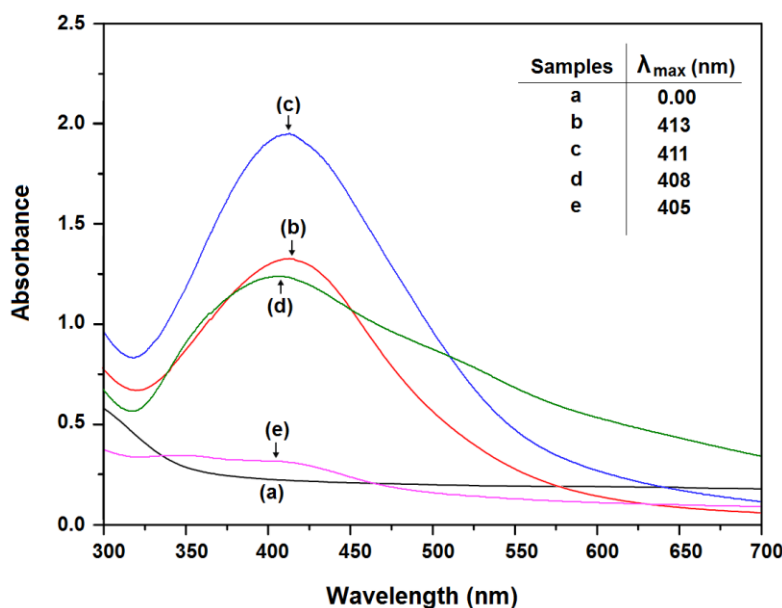


Fig. 1. UV-Vis spectra of (a) RS and (b) through (e) RS/Ag-NCs with 1.0, 5.0, 10.0, and 20.0 wt.% Ag-NPs at different pH values (8.34 to 10.83)

The gradual increase in the percentages of Ag-NPs from 1.0 to 5.0 wt.% resulted in an increase in the intensities of the corresponding peaks between 413 and 411 nm (Fig. 1(b), (c)). However, for Ag-NPs loading from 10.0 to 20.0 wt.%, the intensity of the peaks decreased, which indicated Ag-NPs agglomeration (Fig. 1(d), (e)). The SPR of RS/Ag-NCs prepared at various pH values appeared at 413 nm (pH 8.34), 411 nm (pH 9.16), 408 nm (pH 10.01), and 405 nm (pH 10.83). At low pH values, the UV-Vis spectra of RS/Ag-NCs showed an absorption peak, which appeared in higher wavelengths because of the SPR of Ag-NPs. With increased pH, the peaks were shifted to slightly lower wavelengths, which illustrated the decreased size of Ag-NPs. pH plays a significant role in the shape and size of Ag-NPs (Vanaja *et al.* 2013). The data in this study suggests that a higher pH is more suitable for Ag-NPs synthesis.

Powder X-Ray Diffraction Analysis

Figure 2 illustrates the PXRD patterns of RS and RS/Ag-NCs. In the 2θ angle range of 15 to 25°, the peaks reflected the presence of Ag-NPs. The wide diffraction peak located at 22.20° is related to the RS and showed that the increase in Ag-NPs percentage on the

surface of RS leads to the decrease of the peak intensity in this range. The diffraction profile of all RS/Ag-NCs were similar, and the PXRD peaks at 2θ values of 38.12° , 44.19° , 64.32° , and 77.68° were ascribed to the 111, 200, 220, and 311 crystallographic planes, respectively, of face-centered cubic (fcc) silver crystals, which are distinguished with the Ag-NPs reference code: (01-087-0718). This result suggested that the synthesised Ag-NPs were pure (Shameli *et al.* 2010a).

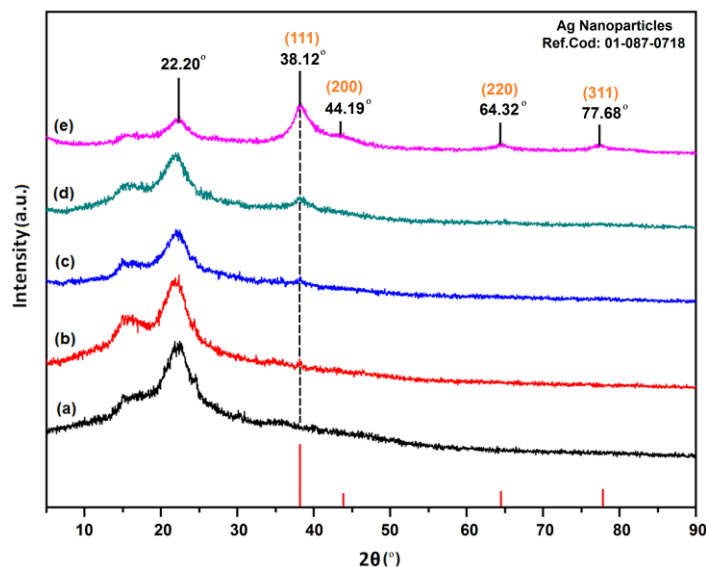


Fig. 2. PXRD of (a) RS and (b through e) RS/Ag-NCs with 1.0, 5.0, 10.0, and 20.0 wt.% Ag-NPs

The pH is important for Ag-NPs synthesis, as it induces reactivity between sodium hydroxide and silver ions. The effect of pH on NPs size was assessed by using various volumes of sodium hydroxide in the reaction. Increased pH led to a reduction in Ag-NPs size, as the repulsion between excess hydroxide ions prevents the growth of crystal particles (Yan *et al.* 2009). Increasing pH also led to a greater net height of RS/Ag-NCs, which is a measure of crystallinity. Therefore, higher crystallinity was obtained at higher pH values, as previously reported (Kamali *et al.* 2012).

The size of the particles (n) was calculated from the PXRD results using the Debye-Scherrer equation, as shown in Eq. 1,

$$n = K\lambda / \beta_{1/2} \cos\theta \quad (1)$$

where K is Scherrer's constant (0.9), λ is the wavelength (1.5418 \AA), $\beta_{1/2}$ is the PXRD peak width at half height, and θ is the Bragg's angle. From Scherrer's equation, the average crystallite size of Ag-NPs for RS/Ag-NCs with 1.0, 5.0, 10.0, and 20.0 wt.% was similar to observations made by TEM (discussed below).

Morphological Studies

Figure 3 presents TEM images and computed histograms of RS/Ag-NCs sizes. The mean diameters and standard deviations of Ag-NPs were 7.37 ± 2.34 , 3.98 ± 2.21 , and 2.50 ± 2.10 nm for 1.0, 10.0, and 20.0 wt.% loading, respectively. As the pH and amount of Ag-NPs on the RS surface increased, the average particle size gradually decreased, and they

dispersed better into the RS matrix. Also, the Ag-NPs had spherical morphologies and a homogeneous distribution.

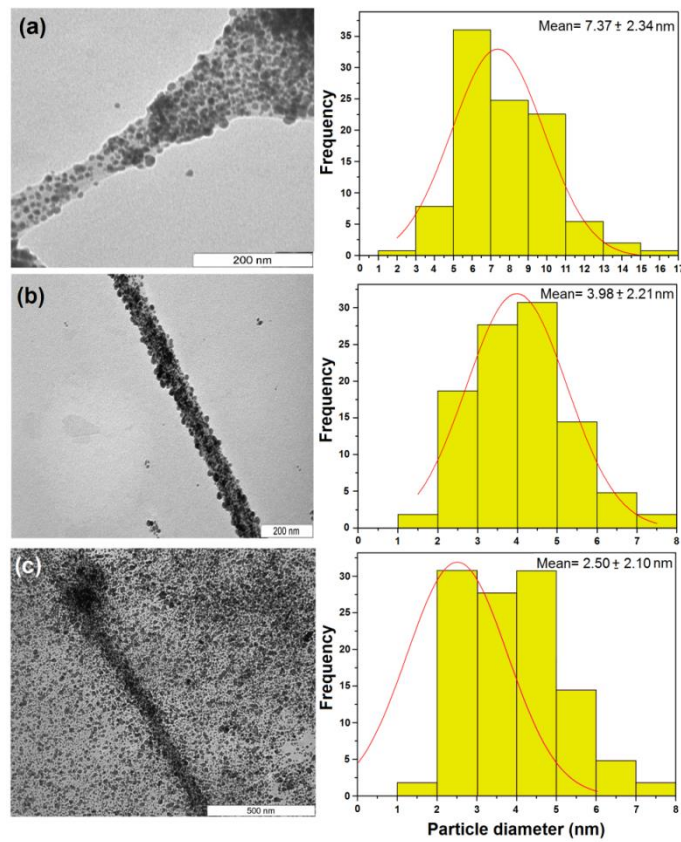


Fig. 3. TEM images and particle size distribution of RS/Ag-NCs with (a) 1.0 wt.%, (b) 10.0 wt.%, or (c) 20 wt.% Ag-NPs

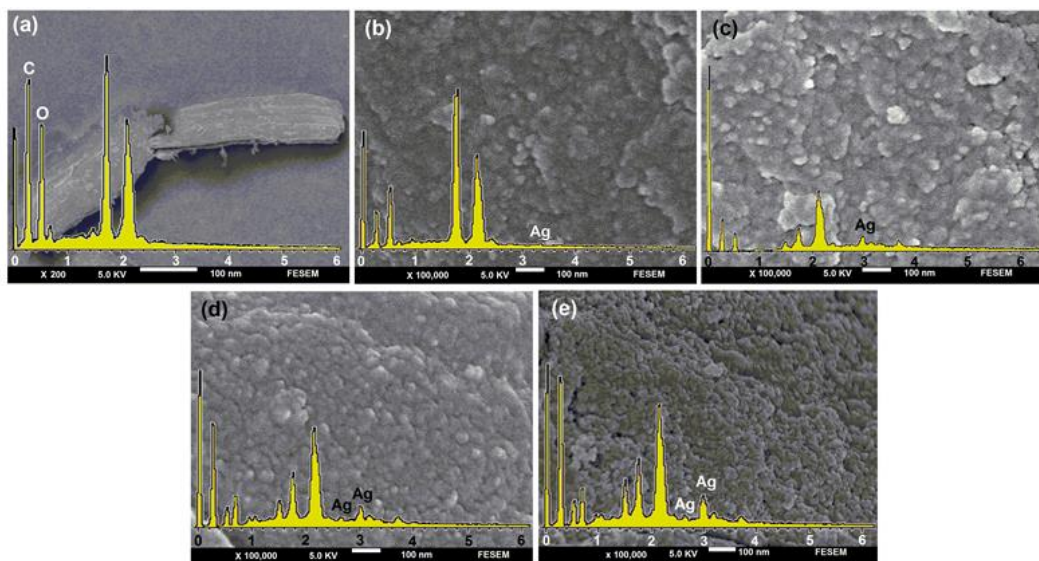


Fig. 4. SEM images and EDX spectroscopy of (a) RS and (b through e) RS/Ag-NCs with 1.0, 5.0, 10.0, and 20.0 wt.% Ag-NPs

The morphology of the RS and RS/Ag-NCs surfaces was also examined by SEM (Fig. 4). RS was not changed after the synthesis of Ag-NPs on its surface. Uniformly prepared RS/Ag-NCs consisted of spherical NPs, which agreed with the TEM images. Increasing the amount of Ag-NPs on the surface of RS caused the particles to aggregate, though they still displayed a desirable distribution. At higher pH values, the Ag-NPs were homogenous and more uniform, and their particle size was smaller.

EDX was used to evaluate the chemical composition of RS and RS/Ag-NCs. In RS (Fig. 4(a)), carbon (C) and oxygen (O) peaks were located at 0.24 keV and 0.4 keV, respectively. After the Ag-NPs were synthesized on the RS surface, Ag peaks were located at 2.7, 3.1, and 3.4 keV in the RS/Ag-NCs (Fig. 4(b through e)) (Bar *et al.* 2009). With increasing Ag-NPs percentage, the intensity of the Ag peaks on the RS surface also increased. Thus, EDX analysis confirmed the deposition of Ag-NPs on the RS surface.

Fourier Transform Infrared Spectra

The FT-IR spectra of RS and RS/Ag-NCs with different concentrations of Ag-NPs are displayed in Fig. 5. In the RS spectrum (Fig. 5(a)), the broad absorption peak located at 3377 cm^{-1} was related to the stretching of -OH groups, and the one located at 2933 cm^{-1} was attributed to C-H stretching vibrations (Chen *et al.* 2011). The smaller bond at 1735 cm^{-1} in the RS was ascribed to aliphatic esters in hemicelluloses or lignin. The peak at 1646 cm^{-1} was related to C=C stretching vibrations (Qin *et al.* 2011). The peak located at 1444 cm^{-1} was assigned to the aromatic C=C stretch of aromatic vibrations in lignin. The peaks from 1363 to 1376 cm^{-1} were attributed to C-H bending. The 1000 to 1200 cm^{-1} region illustrated C-O stretching in cellulose/hemicelluloses (Sun *et al.* 2005b). The peaks placed at 260 to 890 cm^{-1} were assigned to the linkages of glycoside deforming with ring vibration and OH bending (Cao *et al.* 2011).

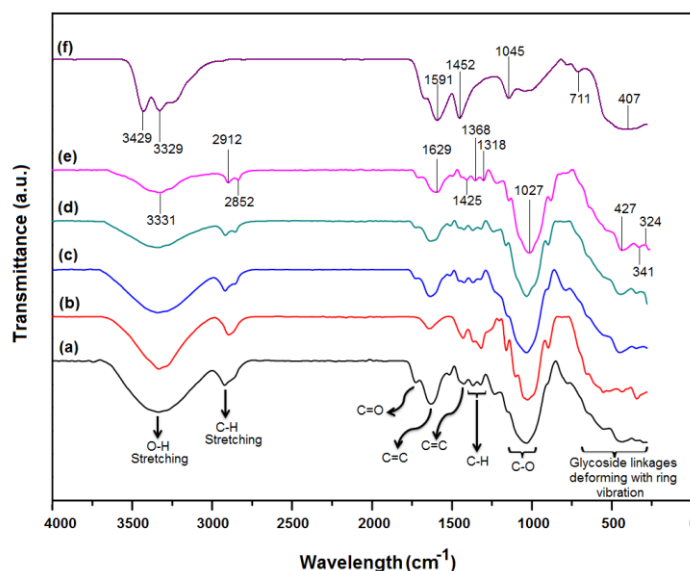


Fig. 5. FT-IR spectra of (a) RS, (b through e) RS/Ag-NCs with 1.0, 5.0, 10.0, and 20.0 wt.% Ag-NPs, and (f) urea

In the urea IR spectrum (Fig. 5(f)), the peaks at 3429 cm^{-1} and 3329 cm^{-1} represented the stretching of $-\text{NH}_2$ groups. The peak at 1591 cm^{-1} was attributed to the N-H group bending vibration and was overlapped with the carbonyl group vibration band.

The peak at 1452 cm^{-1} was related to the stretching of the C-N group. Similar to the increase of the Ag-NP loading percentage, the increase in pH caused the decrease of the peak intensity in all RS/Ag-NCs. This result occurred because when Ag-NPs were prepared on the surface of RS, the raw RS was moderately reduced (Khandanlou *et al.* 2013). All spectra indicated that the interaction among RS, urea, and Ag-NPs occurred through the reduction in the $-\text{OH}$ groups intensity, as there is no chemical bond between them. This result suggests that Ag-NPs were successfully synthesized on the surface of RS. The FT-IR spectrum results were consistent with the XRD results. As the pH increased, the intensity of peaks attributed to raw RS decreased, indicating the presence of Ag-NPs on the RS surface.

Table 1. Inhibition Zone of RS/Ag-NCs

Sample Number	Ag-NPs Loading (%)	Concentration ($\mu\text{g/mL}$)	Inhibition Zone (mm)	
			Gram-positive <i>Staphylococcus aureus</i>	Gram-negative <i>Escherichia coli</i>
1	1	50	10.0	8.5
2	5	50	11.0	9.0
3	10	50	13.0	12.0
4	20	50	15.0	14.0
5	0 (RS)	50	0.0	0.0
6	AgNO_3	50	16.0	15.0

Effect of RS/Ag-NC Size on Antibacterial Activity

As measured *via* the well diffusion technique, RS/Ag-NCs showed noticeable inhibition against *E. coli* and even more so against *S. aureus* (Table 1; Fig. 6). RS alone as a negative control showed no antibacterial activity. The inhibition zone of 5.0% RS/Ag-NCs for *S. aureus* and *E. coli* was 11.0 mm and 9.0 mm, respectively. Although the antibacterial activity was higher for *S. aureus* than *E. coli*, the difference in inhibition zone using *E. coli* from 1.0% to 20.0% (8.5 to 14 mm) was more than for *S. aureus* from 1.0% to 20.0% (10 to 15 mm) RS/Ag-NCs.

The use of Ag-NPs to control the bacterial growth as well as in burns treatment and wound healing has been widely investigated (Boonkaew *et al.* 2014). It has been assumed that the Ag^+ ions bind to the bacterial membrane, which may disintegrate the bacterial morphology. The Ag^+ cations and partially oxidized Ag-NPs have been shown to possess antibacterial activity by either rupturing the negatively charged bacterial cell wall or destabilizing the outer membrane, thereby providing them access to the mitochondria and resulting in the interference with the respiratory chain (You *et al.* 2012).

For all samples, increasing the Ag-NPs surface area, which was the result of the decreasing the particle size from 7.37 to 2.50, led to better and higher antibacterial activity. The smaller nanoparticles have more contact surface area (Pal *et al.* 2007), therefore giving a higher interaction with bacteria and enhance NPs reactivity. Thus, it can be concluded that the bactericidal effect of Ag-NPs is size-dependent (Morones *et al.* 2005). Because of the small size of Ag-NPs, they can penetrate the nuclear content of bacteria with large

surface areas. Thus, their contact with bacteria was the highest, which explains their strong antibacterial effect (Chen *et al.* 2010).

The Ag-NPs antibacterial activity was stronger against *S. aureus* (Gram-positive) than *E. coli* (Gram-negative) (Fig. 6), which was due to structural differences in the bacterial cell walls. Gram-negative bacteria have an exterior layer of lipopolysaccharides, which covers a peptidoglycan layer (Madigan *et al.* 2005); these layers protect the bacteria in hostile environments. Conversely, the cell wall of Gram-positive bacteria contains no lipopolysaccharide layer, such that it is easier for Ag-NPs to penetrate Gram-positive bacteria (Fayaz *et al.* 2010).

Although a clear mechanism for the antibacterial activity of Ag-NPs has not been established so far, several probable mechanisms have been reported. One of the most widely accepted mechanisms is that the positively charged silver ions can interact with negatively charged phosphorus or sulfur-containing biomacromolecular compounds (proteins and nucleic acids), causing structural changes and deformation of bacterial cell walls and membranes that leads to disruption of metabolic processes and followed by cell death (Shankar and Rhim 2015).

It is also believed that the antibacterial activity of silver nanoparticles depends on the surface area of nanoparticles that are most likely to act as reservoirs for releasing the Ag⁺ ions (Feng *et al.* 2000). The antibacterial mechanism of silver nanoparticles has also been suggested to be related to membrane damage due to free radicals derived from the surface of the nanoparticles, causing a significant increase in membrane permeability and leading to cell death (Kim *et al.* 2007).

Figure 7 shows the correlation between the inhibition zone and the percentage and size of Ag-NPs. As the loading percentage of RS/Ag-NCs increased, the inhibition zone increased, which implies a direct relationship between antibacterial activity and Ag-NPs percentage. Additionally, the inhibition zone was increased with decreased Ag-NPs size, which confirmed the inverse relationship between antibacterial activity and Ag-NPs size. In conclusion, increased antibacterial activity was due to the higher surface area of Ag-NPs which is created by decreasing of NPs size.

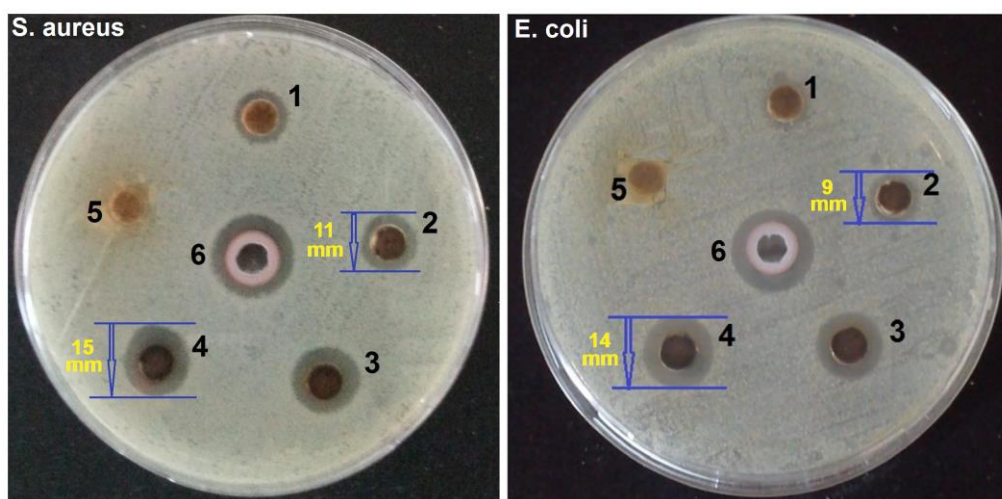


Fig. 6. Inhibition zones of RS/Ag-NCs against Gram-positive (*S. aureus*) and Gram-negative (*E. coli*) bacteria with (1) 1.0, (2) 5.0, (3) 10.0, and (4) 20.0 wt.% Ag-NPs, RS (5), and AgNO₃ (6)

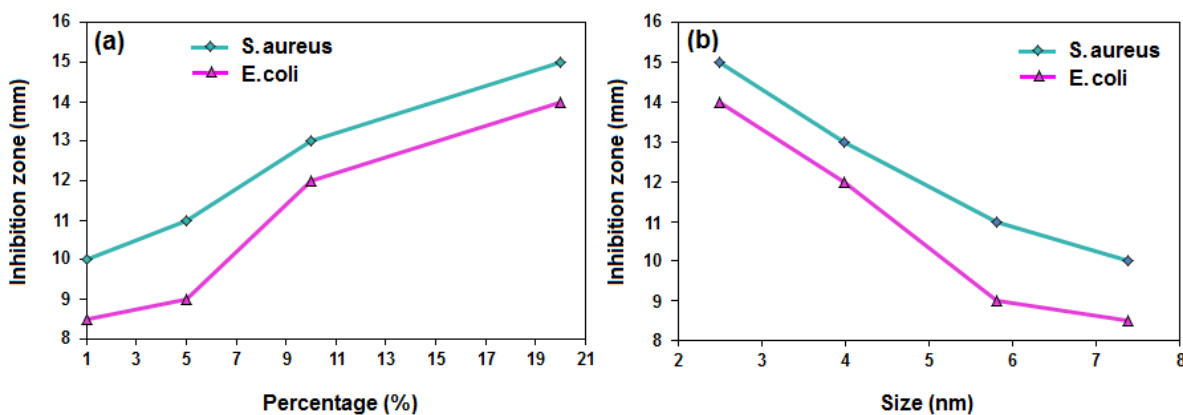


Fig. 7. Antibacterial activity of Ag-NPs of different (a) percentages and (b) sizes

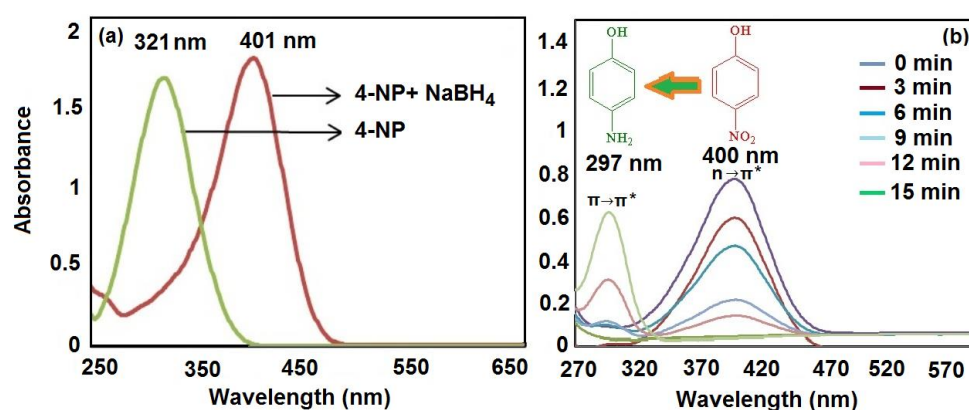


Fig. 8. (a) UV-Vis spectra of 4-NP and alkaline 4-NP by NaBH₄, (b) UV-Vis spectra for the reduction analysis of 4-NP, and (c) proposed mechanism of nitro group reduction catalyzed by 20.0 wt.% RS/Ag-NCs

Catalytic Activity of 20.0 wt.% RS/Ag-NCs and Proposed Mechanism

The catalytic activity of RS/Ag-NCs for hydrogenation of 4-NP was examined. The addition of NaBH₄ into an aqueous solution of 4-NP led to the maximum absorption peak and had a red shift (shifting to the higher wavelength) from 321 to 400 and 401 nm because of the production of 4-nitrophenolate under alkaline conditions (Fig. 8(a)) (Narayanan and Sakthivel 2011). RS/Ag-NCs were added to the aqueous reaction mixtures containing 4-NP and NaBH₄ as the hydrogen donor, and a sample was withdrawn every 3 min to monitor through UV-Vis absorbance (Fig. 8(b)). With the addition of RS/Ag-NCs into the solution, the peak at 400 nm gradually decreased, with the attendant advent of the characteristic peak of the hydrogenation product of 4-aminophenol at approximately 297 nm (Hallett-Tapley *et al.* 2011). This result showed the catalytic activity of Ag-NPs and demonstrated that the RS/Ag-NCs-catalyzed 4-NP hydrogenation had a short induction period (about 3 min in water); the reaction continued to completion within 15 min. Hydrogenation of the nitro compound indicated that it is affected by factors such as electron transfer into the nitro compound and proton accessibility (Kuroda *et al.* 2009). In sum, it is evident that catalytic reduction involves crucial steps including (I) RS/Ag-NCs reaction with borohydride ions to form the metal hydride on the catalyst surface, and (II) the discharge of electrons from BH₄⁻ *via* the metal to the acceptor. Water is a polar protic solvent, and it provides the hydrogen ion required to complete the reduction reaction (Mandlimath and Gopal 2011). Adsorption has a significant role in catalysis. In this study, the RS/Ag-NCs catalyst prepared the adsorption sites for BH₄⁻ ions and for the nitro aromatic compounds, further facilitating electron transfer from the BH₄⁻ ion donor to the nitro aromatic compound acceptor. The proposed mechanism is shown in Fig. 8(c).

CONCLUSIONS

1. This study determined optimal conditions for the synthesis of silver nanoparticles (Ag-NPs) on the rice straw (RS) surface for the first time. The influence of Ag-NPs size on the antibacterial activity of RS/Ag-NCs and the catalytic activity of 20.0 wt.% RS/Ag-NCs were exploited for the reduction of 4-NP in the presence of NaBH₄.
2. The Ag-NPs had spherical morphology, and the size of Ag-NPs on the RS surface with increasing pH from 8 to 10 was decreased from 7.37 to 2.50, which reflected the effect of pH on the size of Ag-NPs.
3. RS/Ag-NCs exhibited strong antibacterial activity against gram-positive (*S. aureus*) and gram-negative (*E. coli*) bacteria. The antibacterial study also indicated that particle size has a significant effect on the inhibitory and bactericidal activities of the as-prepared RS/Ag-NCs. With decreasing nanoparticle size the antibacterial activity was increased.
4. Interestingly, 20.0 wt.% RS/Ag-NCs were found to act as efficient catalysts for the reduction of 4-NP to the corresponding 4-AP in the presence of NaBH₄. The results indicated that the reduction of 4-NP was completed within 15.0 min which implies the high catalytic performance of RS/Ag-NCs.

ACKNOWLEDGEMENTS

The authors thank the University of Malaya for research grants UMRG-RP002B-13AET and RP015C-13AET and High Impact Research Grant HIR- D000015-16001. Moreover, the authors thank the staff of the Department of Chemical Engineering, University Malaya and the Department of Chemistry, University Putra Malaysia, for assistance in this research, especially Dr. Mansor B. Ahmad, as well as the Institute of Bioscience (IBS).

REFERENCES CITED

- Bar, H., Bhui, D. K., Sahoo, G. P., Sarkar, P., De, S. P., and Misra, A. (2009). "Green synthesis of silver nanoparticles using latex of *Jatropha curcas*," *Colloid. Surface A* 339(1–3), 134-139. DOI: 10.1016/j.colsurfa.2009.02.008
- Binod, P., Sindhu, R., Singhanian, R. R., Vikram, S., Devi, L., Nagalakshmi, S., Kurien, N., Sukumaran, R. K., and Pandey, A. (2010). "Bioethanol production from rice straw: An overview," *Bioresour. Technol.* 101(13), 4767-4774. DOI: 10.1016/j.biortech.2009.10.079
- Boonkaew, B., Suwanpreuksa, P., Cuttle, L., Barber, P. M., and Supaphol, P. (2014). "Hydrogels containing silver nanoparticles for burn wounds show antimicrobial activity without cytotoxicity," *J. Appl. Polym. Sci.* 131(9). DOI: 10.1002/app.40215
- Cao, W., Dang, Z., Zhou, X. Q., Yi, X. Y., Wu, P. X., Zhu, N. W., and Lu, G. N. (2011). "Removal of sulphate from aqueous solution using modified rice straw: Preparation, characterization and adsorption performance," *Carbohydr. Polym.* 85(3), 571-577. DOI: 10.1016/j.carbpol.2011.03.016
- Chen, S. F., Li, J. P., Qian, K., Xu, W. P., Lu, Y., Huang, W. X., and Yu, S. H. (2010). "Large scale photochemical synthesis of M@TiO₂ nanocomposites (M=Ag, Pd, Au, Pt) and their optical properties, CO oxidation performance, and antibacterial effect," *Nano Res.* 3(4), 244-255. DOI: 10.1007/s12274-010-1027-z
- Chen, X., Yu, J., Zhang, Z., and Lu, C. (2011). "Study on structure and thermal stability properties of cellulose fibers from rice straw," *Carbohydr. Polym.* 85(1), 245-250. DOI: 10.1016/j.carbpol.2011.02.022
- Das, S., Sasmal, D., Pal, S., Kolya, H., Pandey, A., and Tripathy, T. (2015). "Starch based biodegradable graft copolymer for the preparation of silver nanoparticles," *Int. J. Biol. Macromol.* 81, 83-90. DOI: 10.1016/j.ijbiomac.2015.07.046
- Davarpanah, J., and Kiasat, A. R. (2013). "Catalytic application of silver nanoparticles immobilized to rice husk-SiO₂-aminopropylsilane composite as recyclable catalyst in the aqueous reduction of nitroarenes," *Catal. Commun.* 41, 6-11. DOI: 10.1016/j.catcom.2013.06.020
- De Faria, A. F., Martinez, D. S. T., Stela Maris Meister Meira, S. M. M., de Moraes, A. C. M., Brandelli, A., Filho, A. G. S., and Alves, O. L. (2014). "Anti-adhesion and antibacterial activity of silver nanoparticles supported on graphene oxide sheets," *Colloid. Surface B.* 113, 115-124. DOI: 10.1016/j.colsurfb.2013.08.006

- Fayaz, A. M., Balaji, K., Girilal, M., Yadav, R., Kalaichelvan, P. T., and Venketesan, R. (2010). "Biogenic synthesis of silver nanoparticles and their synergistic effect with antibiotics: A study against gram-positive and gram-negative bacteria," *Nanomed. Nanotech. Biol. Med.* 6(1), 103-109. DOI: 10.1016/j.nano.2009.04.006
- Feng, Q. L., Wu, J., Chen, G. Q., Cui, F. G., Kim, T. N., and Kim, J. O. (2000). "A mechanistic study of the antibacterial effect of silver ions on *Escherichia coli* and *Staphylococcus aureus*," *J. Biomed. Mater. Res.* 52, 662-668. DOI: 10.1002/1097-4636(20001215)52:4<662::AID-JBM10>3.0.CO;2-3
- Gazi, S., and Ananthkrishnan, R. (2011). "Metal-free-photocatalytic reduction of 4-nitrophenol by resin-supported dye under the visible irradiation," *Appl. Catal. B* 105(3-4), 317-325. DOI: 10.1016/j.apcatb.2011.04.025
- Gosheger, G., Harges, J., Ahrens, H., Streitburger, A., Buerger, H., Erren, M., Gonsel, A., Kemper, F. H., Winkelmann, W., and Von Eiff, C. (2004). "Silver-coated megaendoprostheses in a rabbit model—An analysis of the infection rate and toxicological side effects," *Biomaterials* 25(24), 5547-5556. DOI: 10.1016/j.biomaterials.2004.01.008
- Hallett-Tapley, G. L., Crites, C. O. L., González-Béjar, M., McGilvray, K. L., Netto-Ferreira, J. C., and Scaiano, J. (2011). "Dry photochemical synthesis of hydrotalcite, γ -Al₂O₃ and TiO₂ supported gold nanoparticle catalysts," *J. Photoch. Photobio. A* 224(1), 8-15. DOI: 10.1016/j.jphotochem.2011.08.013
- Ibrahim, H. M. (2015). "Green synthesis and characterization of silver nanoparticles using banana peel extract and their antimicrobial activity against representative microorganisms," *J. Radiat. Res. Appl. Sci.* 8(3), 265-275. DOI: 10.1016/j.jrras.2015.01.007
- ISO 16256. (2012). "Clinical laboratory testing and in vitro diagnostic test systems – Reference method for testing the *in vitro* activity of antimicrobial agents against yeast fungi involved in infectious diseases," International Organization for Standardization, Geneva, Switzerland.
- ISO 16782. (2012). "Clinical laboratory testing – Criteria for acceptable lots of dehydrated Mueller-Hinton agar and broth for antimicrobial susceptibility testing," International Organization for Standardization, Geneva, Switzerland.
- ISO/NP 20776-1. (2015). "Clinical laboratory testing and in vitro diagnostic test systems – Susceptibility testing of infectious agents and evaluation of performance of antimicrobial susceptibility test devices - Part 1: Reference method for testing the in vitro activity of antimicrobial agents against rapidly growing aerobic bacteria involved in infectious diseases," International Organization for Standardization, Geneva, Switzerland.
- ISO 20776-1. (2006). "Clinical laboratory testing and *in vitro* diagnostic test systems – Susceptibility testing of infectious agents and evaluation of performance of antimicrobial susceptibility test devices – Part 1: Reference method for testing the in vitro activity of antimicrobial agents against rapidly growing aerobic bacteria involved in infectious diseases," International Organization for Standardization, Geneva, Switzerland.

- ISO 20776-2. (2007). "Clinical laboratory testing and *in vitro* diagnostic test systems – Susceptibility testing of infectious agents and evaluation of performance of antimicrobial susceptibility test devices – Part 2: Evaluation of performance of antimicrobial susceptibility test devices," International Organization for Standardization, Geneva, Switzerland.
- ISO 17511. (2003). "In vitro diagnostic medical devices – Measurement of quantities in biological samples – Metrological traceability of values assigned to calibrators and control materials," International Organization for Standardization, Geneva, Switzerland.
- ISO/NP TS 20914. (2015). "Medical laboratories – Practical guide for the estimation of measurement uncertainty," International Organization for Standardization, Geneva, Switzerland.
- Jana, S., Ghosh, S. K., Nath, S., Pande, S., Praharaj, S., Panigrahi, S., Basu, S., Endo, T., and Pal, T. (2006). "Synthesis of silver nanoshell-coated cationic polystyrene beads: A solid phase catalyst for the reduction of 4-nitrophenol," *Appl. Catal. A-Gen.* 313(1), 41-48. DOI: 10.1016/j.apcata.2006.07.007
- Jeong, S. H., Yeo, S. Y., and Yi, S. C. (2005). "The effect of filler particle size on the antibacterial properties of compounded polymer/silver fibers," *J. Mater. Sci.* 40(20), 5407-5411. DOI: 10.1007/s10853-005-4339-8
- Kamali, M., Ghorashi, S. A. A., and Asadollahi, M. A. (2012). "Controllable synthesis of silver nanoparticles using citrate as complexing agent: Characterization of nanoparticles and effect of pH on size and crystallinity," *Iran. J. Chem. Chem. Eng.* 31(4), 21-28. DOI: 10.21203/rs.3.rs-1021-9986/v1
- Kanmani, P., and Rhim, J. W. (2014). "Physicochemical properties of gelatin/silver nanoparticle antimicrobial composite films," *Food Chem.* 148, 162-169. DOI: 10.1016/j.foodchem.2013.10.047
- Kelly, K. L., Coronado, E., Zhao, L. L., and Schatz, G. C. (2003). "The optical properties of metal nanoparticles: The influence of size, shape, and dielectric environment," *J. Phys. Chem. B* 107(3), 668-677. DOI: 10.1021/jp026731y
- Khan, Z. A., Khan, A., Shah, A., Chen, Y., Wan, P., Khan, A. U., Tahir, K., Muhamma, M., Khan, F. U., and Shah, H. U. (2016). "Photocatalytic, antimicrobial activities of biogenic silver nanoparticles and electrochemical degradation of water soluble dyes at glassy carbon /silver modified past electrode using buffer solution," *J. Photoch. Photobio. B* 156, 100-107. DOI: 10.1016/j.jphotobiol.2016.01.016
- Khandanlou, R., Ahmad, M. B., Shameli, K., and Kalantari, K. (2013). "Investigation of the role of reductant on the size control of Fe₃O₄ nanoparticles on rice straw," *BioResources* 9(1), 642-655. DOI: 10.15376/biores.9.1.642-655
- Kim, J. S., Kuk, E., Yu, K. N., Kim, J. H., Park, S. J., Lee, H. J., Kim, S. H., Park, Y. K., Park, Y. H., and Hwang, C. Y. (2007). "Antimicrobial effects of silver nanoparticles," *Nanomed. Nanotech. Biol. Med.* 3(1), 95-101. DOI: 10.1016/j.nano.2006.12.001
- Kuroda, K., Ishida, T., and Haruta, M. (2009). "Reduction of 4-nitrophenol to 4-aminophenol over Au nanoparticles deposited on PMMA," *J. Mol. Catal. A-Chem.* 298(1-2), 7-11. DOI: 10.1016/j.molcata.2008.09.009
- Kurokochi, Y., and Sato, M. (2015). "Properties of binderless board made from rice straw: The morphological effect of particles," *Ind. Crop. Prod.* 69, 55-59. DOI: 10.1016/j.indcrop.2015.01.044
- Madigan, M. T., Martinko, J. M., Dunlap, P. V., and Clark, D. P. (2005). *Brock Biology of Microorganisms*, Prentice Hall, Upper Saddle River, NJ, USA.

- Mandlimath, T. R., and Gopal, B. (2011). "Catalytic activity of first row transition metal oxides in the conversion of p-nitrophenol to p-aminophenol," *J. Mol. Catal. A-Chem.* 350(1–2), 9-15. DOI: 10.1016/j.molcata.2011.08.009
- Martinez-Castanon, G., Nino-Martinez, N., Martinez-Gutierrez, F., Martinez-Mendoza, J., and Ruiz, F. (2008). "Synthesis and antibacterial activity of silver nanoparticles with different sizes," *J. Nanopart. Res.* 10(8), 1343-1348. DOI: 10.1007/s11051-008-9428-6
- Mohan, S., Oluwafemi, O. S., Songca, S. P., Jayachandran, V.P., Rouxel, D., Joubert, O., Kalarikkal, N., and Thomas, S. (2016). "Synthesis, antibacterial, cytotoxicity and sensing properties of starch-capped silver nanoparticles," *J. Mol. Liq.* 213, 75-81. DOI: 10.1016/j.molliq.2015.11.010
- Mohanram, S., Rajan, K., Carrier, D. J., Nain, L., and Arora, A. (2015). "Insights into biological delignification of rice straw by *Trametes hirsuta* and *Myrothecium roridum* and comparison of saccharification yields with dilute acid pretreatment," *Biomass Bioenergy* 76, 54-60. DOI: 10.1016/j.biombioe.2015.02.031
- Morones, J. R., Elechiguerra, J. L., Camacho, A., Holt, K., Kouri, J. B., Ramirez, J. T., and Yacaman, M. J. (2005). "The bactericidal effect of silver nanoparticles," *Nanotechnology* 16(10), 2346-2353. DOI: 10.1088/0957-4484/16/10/059
- Narayanan, K. B., and Sakthivel, N. (2011). "Synthesis and characterization of nano-gold composite using *Cylindrocladium floridanum* and its heterogeneous catalysis in the degradation of 4-nitrophenol," *J. Hazard. Mater.* 189(1–2), 519-525. DOI: 10.1016/j.jhazmat.2011.02.069
- Oberoi, H. S., Babbar, N., Sandhu, S. K., Dhaliwal, S. S., Kaur, U., Chadha, B., and Bhargav, V. K. (2012). "Ethanol production from alkali-treated rice straw via simultaneous saccharification and fermentation using newly isolated thermotolerant *Pichia kudriavzevii* HOP-1," *J. Ind. Microbiol. Biotechnol.* 39(4), 557-566. DOI: 10.1007/s10295-011-1060-2
- Pal, S., Tak, Y. K., and Song, J. M. (2007). "Does the antibacterial activity of silver nanoparticles depend on the shape of the nanoparticle? A study of the gram-negative bacterium *Escherichia coli*," *Appl. Environ. Microbiol.* 73(6), 1712-1720. DOI: 10.1128/AEM.02218-06
- Qin, L., Qiu, J., Liu, M., Ding, S., Shao, L., Lü, S., Zhang, G., Zhao, Y., and Fu, X. (2011). "Mechanical and thermal properties of poly (lactic acid) composites with rice straw fiber modified by poly (butyl acrylate)," *Chem. Eng. J.* 166(2), 772-778. DOI: 10.1016/j.cej.2010.11.039
- Rashid, M. H., and Mandal, T. K. (2007). "Synthesis and catalytic application of nanostructured silver dendrites," *J. Phys. Chem. C* 111(45), 16750-16760. DOI: 10.1021/jp074963x
- Riboh, J. C., Haes, A. J., McFarland, A. D., Ranjit Yonzon, C., and Van Duyne, R. P. (2003). "A nanoscale optical biosensor: Real-time immunoassay in physiological buffer enabled by improved nanoparticle adhesion," *J. Phys. Chem. B* 107(8), 1772-1780. DOI: 10.1021/jp022130v
- Rosi, N. L., and Mirkin, C. A. (2005). "Nanostructures in biodiagnostics," *Chem. Rev.* 105(4), 1547-1562. DOI: 10.1021/cr030067f
- Rupp, M. E., Fitzgerald, T., Marion, N., Helget, V., Puumala, S., Anderson, J. R., and Fey, P. D. (2004). "Effect of silver-coated urinary catheters: Efficacy, cost-effectiveness, and antimicrobial resistance," *Am. J. Infect. Control.* 32(8), 445-450. DOI: 10.1016/j.ajic.2004.05.002

- Saha, S., Pal, A., Kundu, S., Soumen Basu, S., and Pal, T. (2009). "Photochemical green synthesis of calcium-alginate-stabilized Ag and Au nanoparticles and their catalytic application to 4-nitrophenol reduction," *Langmuir* 26(4), 2885-2893. DOI: 10.1021/la902950x
- Shabanzadeh, P., Yusof, R., and Shameli, K., (2015). "Artificial neural network for modeling the size of silver nanoparticles' prepared in montmorillonite/starch bionanocomposites," *J. Ind. Eng. Chem.* 24, 42-50. DOI: 10.1016/j.jiec.2014.09.007
- Shameli, K., Ahmad, M. B., Yunus, W. M. Z. W., Ibrahim, N. A., Gharayebi, Y., and Sedaghat, S. (2010a). "Synthesis of silver/montmorillonite nanocomposites using γ -irradiation," *Int. J. Nanomed.* 5, 1067-1077. DOI: 10.2147/IJN.S15033
- Shameli, K., Ahmad, M. B., Yunus, W. M. Z. W., Ibrahim, N. A., Rahman, R. A., Jokar, M., and Darroudi, M. (2010b). "Silver/poly (lactic acid) nanocomposites: Preparation, characterization, and antibacterial activity," *Int. J. Nanomed.* 5, 573-579. DOI: 10.2147/IJN.S12007
- Shankar, S., and Rhim, J. W. (2015). "Amino acid mediated synthesis of silver nanoparticles and preparation of antimicrobial agar/silver nanoparticles composite films," *Carbohydr. Polym.* 130, 353-363. DOI: 10.1016/j.carbpol.2015.05.018
- Shrivastava, S., Bera, T., Singh, S. K., Singh, G., Ramachandrarao, P., and Dash, D. (2009). "Characterization of antiplatelet properties of silver nanoparticles," *ACS Nano*. 3(6), 1357-1364. DOI: 10.1021/nn900277t
- Solanki, J. N., and Murthy, Z. V. P. (2011). "Reduction of nitro aromatic compounds over Ag/Al₂O₃ nanocatalyst prepared in water-in-oil microemulsion: Effects of water-to-surfactant mole ratio and type of reducing agent," *Ind. Eng. Chem. Res.* 50(12), 7338-7344. DOI: 10.1021/ie200536q
- Sondi, I., and Salopek-Sondi, B. (2004). "Silver nanoparticles as antimicrobial agent: A case study on *E. coli* as a model for Gram-negative bacteria," *J. Colloid Interf. Sci.* 275(1), 177-182. DOI: 10.1016/j.jcis.2004.02.012
- Sun, R. W. Y., Chen, R., Chung, N. P. Y., Ho, C. M., Lin, C. L. S., and Che, C. M. (2005a). "Silver nanoparticles fabricated in Hepes buffer exhibit cytoprotective activities toward HIV-1 infected cells," *Chem. Commun.* 2005, 5059-5061. DOI: 10.1039/B510984A
- Sun, X., Xu, F., Sun, R., Fowler, P., and Baird, M. (2005b). "Characteristics of degraded cellulose obtained from steam-exploded wheat straw," *Carbohydr. Res.* 340(1), 97-106. DOI: 10.1016/j.carres.2004.10.022
- Tao, A., Sinsersuksakul, P., and Yang, P. (2007). "Tunable plasmonic lattices of silver nanocrystals," *Nat. Nanotechnol.* 2, 435-440. DOI: 10.1038/nnano.2007.189
- Vanaja, M., Rajeshkumar, S., Paulkumar, K., Gnanajobitha, G., Malarkodi, C., and Annadurai, G. (2013). "Kinetic study on green synthesis of silver nanoparticles using *Coleus aromaticus* leaf extract," *Adv. Appl. Sci. Res.* 4(3), 50-55.
- Wang, Z., Xu, C., Li, X., and Liu, Z. (2015). "In situ green synthesis of Ag nanoparticles on teapolyphenols-modified graphene and their catalytic reduction activity of 4-nitrophenol," *Colloid. Surface A* 485, 102-110. DOI: 10.1016/j.colsurfa.2015.09.015

- Yan, H., Zhang, J., You, C., Song, Z., Yu, B., and Shen, Y. (2009). "Influences of different synthesis conditions on properties of Fe₃O₄ nanoparticles," *Mater. Chem. Phys.* 113(1), 46-52. DOI: 10.1016/j.matchemphys.2008.06.036
- You, C., Han, C., Wang, X., Zheng, Y., Li, Q., Hu, X., and Sun, H. (2012). "The progress of silver nanoparticles in the antibacterial mechanism, clinical application and cytotoxicity," *Mol. Biol. Rep.* 39(9), 9193-9201. DOI: 10.1007/s11033-012-1792-8
- Zheng, Y., Zhu, Y., Tiana, G., and Wang, A. (2015). "In situ generation of silver nanoparticles within crosslinked 3D guar gum networks for catalytic reduction," *Int. J. Biol. Macromol.* 73, 39-44. DOI: 10.1016/j.ijbiomac.2014.11.007

Article submitted: December 7, 2015; Peer review completed: February 6, 2016; Revised version received: February 21, 2016; Accepted: February 22, 2016; Published: March 3, 2016.

DOI: 10.15376/biores.11.2.3691-3708